LAWRENCE
LIVERMORE
NATIONAL
LABORATORY

LLNL-JRNL-404764

# Deep mantle contributions to the surface dynamics of the North American continent

A. M. Forte, R. Moucha, N. A. Simmons, S. P. Grand, J. X. Mitrovica

June 19, 2008

Tectonophysics

## Disclaimer

Elsevier Editorial System(tm) for Tectonophysics
Manuscript

Manuscript Number: TECTO6287

Title: Deep mantle contributions to the surface dynamics of the North American continent

Article Type: Special Issue: Pasy Artem Lithosphere

Keywords: North America; continental dynamics; seismic tomography; mantle convection; mantle viscosity; dynamic topography; gravity anomalies; Kula-Farallon; lower mantle

Corresponding Author: Professor Alessandro Forte,

Corresponding Author's Institution: Université du Québec à Montréal

First Author: Alessandro Forte

Order of Authors: Alessandro Forte; Robert Moucha; Nathan Simmons; Stephen Grand; Jerry Mitrovica

Abstract: The regional and continental scale dynamics of North America and vicinity are explored using a high resolution model of mantle flow. The model is constrained by simultaneously inverting global seismic and mantle-convection data sets and it includes an explicit treatment of the positive chemical buoyancy of the continental tectosphere. Moreover, it adopts a depth dependent mantle viscosity structure which reconciles both glacial isostatic adjustment (GIA) and convection data. The flow model successfully reproduces plate velocities and observations of surface gravity and topography, including the continent-scale quasi-linear depression (after corrections for GIA and crustal heterogeneity) extending from northern Alaska to Venezuela. The predictions also match lithospheric flow and stress fields inferred from local and regional measurements of seismic anisotropy and surface deformation. We demonstrate that these signals are largely driven by viscous flow coupled to density anomalies in the deep portions of the upper mantle and within the lower mantle, where the latter may be associated with the descent of the ancient Kula-Farallon plate system and an active mantle upwelling below the Pacific. More importantly, the flow calculations elucidate how these large-scale heterogeneities give rise to regional-scale flow and stress patterns below the southwestern U.S. and below the central U.S.

This work performed under the auspices of the U.S. Department of Energy by Lawrence Livermore National Laboratory under Contract DE-AC52-07NA27344.

Tectonophysics 000 (2008) 0–0

# Deep mantle contributions to the surface dynamics of the North American continent

A.M. Forte[a], R. Moucha[a], N.A. Simmons[b], S.P. Grand[c], J. X. Mitrovica[d]

[a] *GEOTOP – Dept. Sci. Terre & Atmosphère, Université du Québec à Montréal, Montréal QC, H3C 3P8 Canada*

[b] *Atmospheric, Earth & Energy Division, Lawrence Livermore National Laboratory, Livermore CA, 94551 USA*

[c] *Jackson School of Geosciences, University of Texas at Austin, Austin TX, 78712 USA*

[d] *Dept. of Physics, University of Toronto, Toronto ON, M5S 1A7 Canada*

**Abstract**

The regional and continental scale dynamics of North America and vicinity are explored using a high resolution model of mantle flow. The model is constrained by simultaneously inverting global seismic and mantle-convection data sets and it includes an explicit treatment of the positive chemical buoyancy of the continental tectosphere. Moreover, it adopts a depth dependent mantle viscosity structure which reconciles both glacial isostatic adjustment (GIA) and convection data. The flow model successfully reproduces plate velocities and observations of surface gravity and topography, including the continent-scale quasi-linear depression (after corrections for GIA and crustal heterogeneity) extending from northern Alaska to Venezuela. The predictions also match lithospheric flow and stress fields inferred from local and regional measurements of seismic anisotropy and surface deformation. We demonstrate that these signals are largely driven by viscous flow coupled to density anomalies in the deep portions of the upper mantle and within the lower mantle, where the latter may be associated with the descent of the ancient Kula-Farallon plate system and an active mantle upwelling below the Pacific. More importantly, the flow calculations elucidate how these large-scale heterogeneities give rise to regional-scale flow and stress patterns below the southwestern U.S. and below the central U.S.

**Key words:** North America, continental dynamics, seismic tomography, mantle flow, mantle viscosity, dynamic topography, gravity anomalies, Kula-Farallon, lower mantle.

## 1 INTRODUCTION

The nature and extent of coupling between continental dynamics and mantle convection is an outstanding problem in geodynamics which has been extensively explored over the past three decades (Jordan 1975; Alvarez 1982; Alvarez 2001; Gurnis 1988; Bird 1998; Lowman & Jarvis 1999; Sleep 2005). North America is a continent exhibiting strong geophysical and geological contrasts between the older, slowly deforming eastern half (Gan & Prescott 2001) and the young, tectonically active western half (Flesch et al. 2000; Zandt et al. 2004). The extent to which the North American continent is coupled to mantle flow and the depth range in the mantle which contributes to the surface dynamics is a fundamental question which has been investigated in a variety of studies (Zoback & Zoback 1980; Gough 1984; Bokelmann 2002a; Liu & Bird 2002), but a comprehensive understanding of the underlying thermal convection dynamics and its impact on surface observables remains elusive.

Mantle flow dynamics below North America are manifested in a wide variety of surface geological and geophysical phenomena, such as: tectonic provinces and geochronological ages (Hoffman 1988; Hoffman 1990), mantle xenoliths and heat flow (Rudnick et al. 1998; Russell & Kopylova 1999; Canil et al. 2003), topography and gravity anomalies (Bechtel et al. 1990; Perry et al. 2003), crustal stress and intraplate seismicity (Zoback & Zoback 1980; Gough et al. 1983; Du et al. 2003). Numerical models based on thin sheet formulations have employed these surface constraints to infer the state of stress and deformation in the deep continental crust and lithosphere (Richardson & Reding 1991; Liu & Bird 2002). These models make a variety of assumptions concerning stress boundary conditions and large uncertainties remain concerning the pattern of mantle flow and the azimuth of convection induced stresses acting on the base of the North American lithosphere.

Constraints on the deep structure below North America have been provided by seismic tomographic imaging (Grand 1994; van der Lee & Nolet 1997; Godey et al. 2003; Nettles & Dziewonski

2008). Although such images can yield maps of present-day thermal structure in the upper mantle (Forte & Perry 2000; Goes & van der Lee 2002; Perry et al. 2003; Godey et al. 2004) they cannot directly provide any information on the pattern of sub-continental mantle flow. Inferences of the lithospheric deformation field below North America can be derived from seismic anisotropy measurements (Silver & Chan 1991) and they have been interpreted in terms of mantle flow directions (Fouch et al. 2000; Silver & Holt 2002; Gök et al. 2003; Becker et al. 2006). Seismic anisotropy has also been interpreted in terms of coupling stresses between the continental lithosphere and asthenosphere below the Canadian Shield (Bokelmann 2002b). The connection between seismic anisotropy and the mantle flow field is, however, indirect and depends on the assumed deformation history of the mantle region under study (Kaminski & Ribe 2001). Furthermore, the degree of hydration in the mantle under tectonically active regions, such as the western half of North America (Dixon et al. 2004), may significantly alter the relation between mantle flow and seismic anisotropy (Jung & Karato 2001). In addition to these complexities, there remains the basic problem of the limited geographical coverage of the seismic anisotropy measurements.

A uniform, direct mapping of the mantle flow and stress fields below North America can be obtained from viscous flow models of the mantle (Richards & Hager 1984; Ricard et al. 1984; Forte & Peltier 1987) which incorporate mantle buoyancy forces derived from seismic tomography models. These flow models have previously been used to explain the origin of surface gravity and topography anomalies on North America (Pari & Peltier 2000; Perry et al. 2003; Forte et al. 2007; Moucha et al. 2008) and on continents globally (Forte & Perry 2000). Tomography-based flow models have also provided predictions of buoyancy driven tectonic plate motions (Ricard & Vigny 1989; Forte & Peltier 1991) and lithospheric stresses (Steinberger et al. 2001; Lithgow-Bertelloni & Guynn 2004) which agree well with the present-day plate velocities and global stress compilations.

In the following we build on recent advances in imaging 3-D mantle structure by simultaneously inverting global seismic and geodynamic data (Forte & Grand 2003; Simmons et al. 2006) in order to provide improved constraints on the pattern and amplitude of surface gravity and topography anomalies and their relationship to the flow and stress fields below North America. Recent

work (Forte et al. 2007; Moucha et al. 2008) has identified the significant mantle dynamic impact, as measured in terms of dynamic topography and stress, arising from the descent of the ancient Farallon slab under North America. In the present study we explore in detail the depth intervals in the mantle that provide the greatest contribution to the convection-related surface observations. As we show below, the buoyancy forces located deep below the surface, at depths in excess of 400 km, provide strong contributions to the surface dynamics of North America.

## 2 GEODYNAMIC RESPONSE FUNCTIONS FOR A VISCOUS MANTLE

The first fundamental input required in a calculation of viscous flow in the mantle is a model of the rheological structure of the mantle. Details of the viscous flow theory may be found elsewhere (Richards & Hager 1984; Forte 2007) and it suffices to point out that the flow calculations presented below are obtained on the basis of a gravitationally consistent, compressible-flow theory in which rigid tectonic plates are coupled to the buoyancy-driven mantle flow (Forte & Peltier 1991; Forte & Peltier 1994). Alternative treatments of plate coupling have been proposed (Ricard & Vigny 1989; Gable et al. 1991), and in all cases the underlying principle is that surface plate motions must be predicted on the basis of the integrated buoyancy forces in the mantle. The plate motions must not be imposed as an a-priori surface-velocity boundary condition. All calculations presented below adhere to the fundamental requirement that the plate motions are driven solely by mantle buoyancy forces.

The rheological structure of the mantle is represented in terms of a depth-dependent effective viscosity. The viscosity profile employed here (Fig. 1a) is derived from a simultaneous inversion of global convection-related surface data (free-air gravity anomalies, dynamic surface topography, tectonic plate motions, excess core-mantle boundary ellipticity) and glacial isostatic adjustment (GIA) data consisting of post-glacial decay times from Laurentia and Fennoscandia as well as a revised Fennoscandian relaxation-time spectrum (Mitrovica & Forte 2004). This viscosity profile provides a very good fit to both families of data, despite the very different spatial and temporal scales which characterise the convection and GIA observables.

Once an appropriate model of the mantle viscosity structure has been selected, it is possible to

calculate the flow-induced response of the mantle for an arbitrary distribution of internal density anomalies. This theoretical relationship between the mantle density anomalies and the principal convection related surface observables (i.e., geoid or gravity anomalies, dynamic surface topography, plate motions) may be summarised in terms of geodynamic response or kernel functions (Hager & Clayton 1989). This relationship is usually expressed in the spectral domain defined by spherical harmonic basis functions and it characterises the response of the mantle to internal density loads $\delta\rho$ of different horizontal wavelengths, as follows:

$$\delta O_\ell^m = f_\ell \int_{r_{cmb}}^{r_{surf}} K_\ell(r)\ (\delta\rho)_\ell^m(r)\,\mathrm{d}r \tag{1}$$

in which $(\delta\rho)_\ell^m(r)$ and $\delta O_\ell^m$ are the spherical harmonic coefficients of the internal density anomalies and of the geodynamic observable (e.g., geoid or free-air gravity anomalies, dynamic topography), respectively, $K_\ell(r)$ is the corresponding kernel function and $f_\ell$ is a factor which depends on the geodynamic observable. On a spherical surface of radius $r$, a spherical harmonic degree $\ell$ corresponds to horizontal wavelength $\lambda_\ell$ given by the following expression:

$$\lambda_\ell = \frac{2\pi r}{\sqrt{\ell(\ell+1)}} \tag{2}$$

For example, at the Earth's surface $\ell = 2$ and 32 correspond to an equivalent horizontal length scale (or half wavelength) of about 8,000 and 600 km, respectively.

On the basis of the method employed here for modeling mantle flow with rigid surface plates (Forte & Peltier 1994; Forte 2007), one can show that the internal density perturbations $\delta\rho$ in the mantle may be geometrically separated into two complementary parts:

$$\delta\rho(r,\theta,\phi) = \delta\hat{\rho}(r,\theta,\phi) + \delta\bar{\rho}(r,\theta,\phi)\ . \tag{3}$$

The surface flow field produced by $\delta\hat{\rho}$ is entirely compatible with the allowable rigid-body rotations of the tectonic plates and thus it is modelled with a free-slip surface boundary condition (the plates fully participate in the underlying flow generated by $\delta\hat{\rho}$). In contrast the surface flow field produced by $\delta\bar{\rho}$ cannot be represented by any rigid-body rotations of the plates and is in fact 'orthogonal' to the vector space of all allowable plate motions. The flow field driven by $\delta\bar{\rho}$ is thus modelled with a no-slip surface boundary condition.

On the basis of equation (3), a mantle flow model which incorporates coupling to rigid surface

plates requires the use of geodynamic response functions $K_\ell(r)$ in (1) for both free-slip and no-slip surface boundary conditions. These geodynamic kernels calculated on the basis of the viscosity profile in Fig. 1a are illustrated in Fig. 1b–d. Comparing the free-slip and no-slip gravity kernels (Fig. 1c), we note that the largest contribution from density anomalies in the top half of the mantle is provided by those anomalies $\delta\hat{\rho}$ which are efficient in driving observable plate motions (Fig. 1b). These anomalies correspond to subducting slabs and upper-mantle plumes below the mid-ocean ridges. In the bottom half of the mantle the density anomalies belonging to the $\delta\bar{\rho}$ family provide the largest contribution to the surface geoid or gravity anomalies. At sufficiently short horizontal wavelengths (corresponding to harmonic degrees $\ell \geq 16$) we note that the distinction between $\delta\hat{\rho}$ and $\delta\bar{\rho}$ anomalies begins to disappear and both provide equal contributions to the surface observables.

## 3 JOINT SEISMIC-GEODYNAMIC CONSTRAINTS ON MANTLE DENSITY AND CONTINENTAL ROOT BUOYANCY

The second most important input in a calculation of the mantle convective flow is a description of the internal density anomalies which provide the driving buoyancy forces. In this study, mantle density perturbations $\delta\rho$ are derived from a 3-D distribution of shear-wave velocity anomalies $\delta V_S$ obtained from a new joint inversion of global seismic and geodynamic data (Simmons et al. 2006), where the latter are interpreted in terms of whole-mantle flow. This seismic tomography model, called 'TX05WM', is parameterised in terms of blocks that are approximately 250 km in each lateral dimension and vary from 75 to 150 km in thickness, yielding a total of 22 depth layers from the surface to the core-mantle boundary (CMB). For the purposes of the dynamical flow calculations, the lateral heterogeneity in model TX05WM is expanded in spherical harmonics up to degree 32. All convection-related surface data sets are also represented by harmonics up to degree 32.

At shallow depths (down to about 150 km) the seismic structure of North America in model TX05WM (Fig. 2) is dominated by the contrast between the very slow western margin of North America and the much faster eastern and central portion of the continent. Below the continental

high-velocity root, centred under the Canadian Shield at a depth of about 250 km, there is a transition to shorter-wavelength structures, notably the slow-velocity anomaly below the Pacific Ocean just off the coast of the southwestern U.S. and a similar slow-velocity structure centred below Hudson Bay (depths 400 – 1000 km in Fig. 2). At the bottom of the transition-zone region (depths $>$ 600 km in Fig. 2) quasi-linear high-velocity anomalies begin to appear below the central and eastern U.S. and they extend to great depths into the lower mantle. As will be shown below, each of these deep-seated high- and low-velocity structures makes a major impact on mantle dynamics below North America.

The connection between the density and seismic anomalies, expressed in terms of a logarithmic scaling ratio $\mathrm{dln}\,\rho/\mathrm{dln}\,\mathrm{V_S}$, may be estimated on the basis of mineral physics data if it is assumed that temperature anomalies are the dominant source of lateral heterogeneity in the mantle (Karato & Karki 2001; Cammarano et al. 2003). In cases where significant chemical heterogeneity may be superimposed on thermal heterogeneity, the density-velocity scaling may instead be derived by inverting surface geodynamic constraints on mantle density (Forte & Perry 2000; Forte & Mitrovica 2001).

Seismically imaged roots below continental shield regions are expected to have a thermal and chemical structure which is distinctly different from the mantle under ocean basins (Jordan 1981). Such lateral variations in chemical composition imply that the density-velocity scaling factor $\mathrm{dln}\,\rho/\mathrm{dln}\,\mathrm{V_S}$ must also vary laterally between the continental roots and ambient mantle. It is therefore necessary to explicitly identify the seismic anomalies below continental shields, $(\delta V_S)_{shield}$, which are characterised by anomalously fast shear wave velocities, and seismic anomalies in the ambient mantle, $(\delta V_S)_{thermal}$, which are assumed to be mainly thermal in origin. The density perturbations are then a sum of 'shield' anomalies below continents and 'thermal' anomalies in the ambient mantle, as follows:

$$\frac{\delta\rho}{\rho} = \left(\frac{\mathrm{dln}\,\rho}{\mathrm{dln}\,\mathrm{V_S}}\right)_{shield}\left(\frac{\delta V_S}{V_S}\right)_{shield} + \left(\frac{\mathrm{dln}\,\rho}{\mathrm{dln}\,\mathrm{V_S}}\right)_{thermal}\left(\frac{\delta V_S}{V_S}\right)_{thermal} \tag{4}$$

The density-velocity scaling coefficients for shield and thermal mantle (Fig. 3) are obtained by inverting all convection-related surface data (plate velocities, free-air gravity anomalies, dynamic topography, excess CMB ellipticity) which directly constrain the density perturbations in

the mantle. Complete details of the density inversion procedure and surface data sets are presented in Perry et al. (2003). The inversions are carried out in the context of a viscous flow calculation based on tomography model TX05WM (Fig. 2) and using the geodynamic kernels based on the joint convection-GIA viscosity profile (Fig. 1). In addition to the important crustal corrections for continental dynamic topography (Perry et al. 2002), the gravity anomalies over North America have been corrected by removing the GIA contribution. The non-isostatic topography data are also corrected for the incomplete post-glacial rebound of the Hudson Bay region. These GIA corrections are predicted on the basis of the viscosity profile in Fig. 1a and the corrected North American gravity and dynamic topography fields are shown in Fig. 4a,b.

The heterogeneity associated with subcontinental roots below the shields, $(\delta V_S)_{shield}$, is characterised by a density-velocity scaling coefficient (Fig. 3, solid blue curve) which differs strongly from that of the ambient mantle (Fig. 3, solid red curve) in the upper 200 km of the mantle. The negative sign of the shield scaling in the top 100 km implies that the shallow, seismically fast cratonic mantle is buoyant ($\delta\rho < 0$) and must therefore be strongly depleted in its basaltic constituents (Jordan 1981). The depth resolution of the buoyant region (in layer 1 in model TX05WM) is limited by the relatively coarse vertical parameterisation of the tomography model. Xenoliths derived from Archaean continental mantle (Poudjom Djomani et al. 2001) provide independent support for the geodynamic inference of chemical buoyancy in the top half of the continental roots. On the basis of the intersection between the shield and thermal scaling coefficients (Fig. 3), the depth of the chemical boundary layer hypothesized by Jordan (Jordan 1981) is inferred to be approximately 200 km.

The isopycnic hypothesis (Jordan 1978) suggests that chemical and thermal contributions to density perturbations are balanced so that continental roots are neutrally buoyant. This hypothesis may be tested by inverting the convection-related data for the optimal scaling coefficient in the ambient mantle, $(\mathrm{d}\ln\rho/\mathrm{d}\ln \mathrm{V_S})_{\mathrm{thermal}}$, with the a-priori constraint of a zero value for the shield scaling coefficient. The result (Fig. 3, dashed red curve) differs slightly from the thermal scaling obtained in the previous inversion but, as shown below, the isopycnic hypothesis is less successful

in fitting the dynamic topography data. Recent investigations of combined gravity, thermal and seismic data have also shown that the isopycnic hypothesis is problematic (Kaban et al. 2003).

## 4 DEEP-MANTLE SIGNATURE IN SURFACE DATA

Table 1 provides a quantitative summary of the agreement between the convection-related data and the corresponding predictions delivered by the viscous flow calculation based on the new joint tomography model TX05WM. The good matches to the plate motions and gravity anomalies, in North America and globally, over the entire range of harmonics up to degree 32, are a substantial improvement over previous tomography-based flow calculations (Perry et al. 2003; Forte & Mitrovica 2001). The match to the dynamic topography is less than the gravity fit and this may in part be due to the significant uncertainties in the crustal heterogeneity model which has been employed in the isostatic topography correction (Perry et al. 2002). The tabulated results show that the isopycnic hypothesis yields a poorer fit to the dynamic topography data.

Predicted gravity and dynamic topography variations in North America (Fig. 4c,d) match the surface data (Fig. 4a,b) very well. A large scale, quasi linear mid-continental depression (MCD) extending from northern Alaska to the southern Caribbean is clearly discernible in the gravity and topography fields, especially in the predictions shown in Fig. 4c,d. This MCD (identified by dashed lines in Figs. 4b,d,f) lies above a similarly extended, high seismic velocity structure in the lower mantle which has been identified as the descending Farallon slab (Grand et al. 1997). The approximate position and descent history of this large tabular anomaly has also been estimated on the basis of mantle convection models which incorporate paleomagnetic reconstructions of Cenozoic plate motions (Lithgow-Bertelloni & Richards 1998; Bunge & Grand 2000).

In view of the potential Farallon slab signature in the surface gravity and topography fields, it is of interest to explore and quantify the relative importance of deep-mantle contributions to the convection-related surface data. To this end, a viscous flow calculation has been carried out in which all density anomalies in the top 400 km of the mantle have been set to zero. The impact of this operation on the predicted North American gravity field (Fig. 4e) is minimal, thereby confirming the dominance of deep-mantle contributions to this field. The predicted dynamic topography

(Fig. 4f) shows a greater change, owing the non-negligible contribution of asthenospheric density anomalies, but it is still clear that deep-mantle sources below 400 km depth provide a significant contribution to North American topography and produce a peak mid-continental depression of about 600 m (compared to the total value of about 1000 m in Fig. 4d). Indeed, the region of depressed topography in Fig. 4f is closely correlated with the outline of the former Western Interior Seaway (Ziegler et al. 1985; Kauffman 1988). The Cretaceous subsidence which lead to the creation of this seaway, and the subsequent Tertiary uplift, has previously been modelled in terms of long wavelength continental tilting produced by time dependent subduction along the west coast of North America (Mitrovica et al. 1989; Lithgow-Bertelloni & Gurnis 1997).

Table 1 also summarises the fits and mean amplitudes of the predicted surface observables for a number of scenarios, where density anomalies are removed in the top 400 and 670 km of the mantle. The alternative scenario in which all density anomalies in the lower mantle are removed, is also included (last row, Table 1). From these tabulations it is evident that even in the extreme case where all density anomalies in the upper mantle are eliminated, the predicted surface observables have amplitudes which are more than 60% of the total predicted values.

## 5 DEEP-MANTLE CONTRIBUTIONS TO FLOW AND STRESS BELOW NORTH AMERICA

The viscous flow model used to predict the surface observables in Fig. 4 also yields maps of buoyancy induced flow directions below North America (Fig.5). This flow model is dynamically coupled to rigid rotating surface plates, in a no-net-rotation reference frame, and it provides a nearly perfect match (Table 1) to the present-day plate motions (Argus & Gordon 1991). The predicted flow at the base of the lithosphere (Fig. 5a) is closely correlated to the observed surface plate velocities. However, in the asthenosphere (Fig. 5b) there is a significant change in the horizontal flow trajectories, particularly beneath the western half of North America. Such a rapid change with depth, facilitated by reduced mantle viscosity at the base of the lithosphere (Fig. 1a), yields a flow field which is consistent with independent estimates of asthenospheric flow below the western U.S. deduced from anisotropy and surface deformation data (Silver & Holt 2002).

Below the North American shield, vertical flow rates are negligible (Fig. 5a), as would be expected on the basis of the inferred positive buoyancy of the top half of the continental root (Fig. 3). The most pronounced centres of downwelling in the asthenosphere (Fig. 5b) are located below the Aleutian, Central American and Caribbean trenches, and the central portion of the U.S. These downwellings increase in strength at the top of the transition zone region (Fig. 5c). Moreover, at the base of the upper mantle (Fig. 5d), the individual zones of downwelling merge to form an arc of strong, descending flow that extends from Alaska, through the central U.S. and into the Caribbean. This flow pattern is largely driven by subduction of the Kula-Farallon plates in the lower mantle (see below); we note, in this regard, that the surface dynamic topography driven by deep-mantle sources (Fig. 4f) is well correlated with the pattern of vertical flow at 670 km depth (Fig. 5d).

East-north-easterly horizontal flow below the south-western US, accompanied by vertical upwelling in the same region, is present at all depths below the lithosphere (Fig. 5). This flow pattern which is driven by both the descending Farallon slab and by a large-scale upwelling below the Pacific ocean, to the southwest of the Gulf of California (Fig. 5c), was first envisaged two decades ago (Gough 1984) on the basis of surface stress patterns (Zoback & Zoback 1980). A similar pattern of vertical and horizontal flow, but on a more reduced spatial scale, is also occurring below the Juan de Fuca plate (Fig. 5b,c). The pattern of sub-lithospheric horizontal flow off the western coast of Central America, characterised by an apparent eastward 'jet' below the Caribbean (Fig. 5c) is in accord with the flow patterns hypothesized more than 2 decades ago (Alvarez 1982; Alvarez 2001).

The geographical expression of buoyancy driven forces acting on the base of the lithosphere is similar to that of the flow field. We quantify the convection-induced drag forces in terms of traction vectors $\mathbf{t} = \mathbf{T} \cdot \hat{\mathbf{n}}$, where $\mathbf{T}$ is the viscous stress tensor and $\hat{\mathbf{n}}$ is the unit vector directed radially inwards. In the calculation of the viscous stress tensor we also include all contributions arising from the dynamic pressure perturbations in addition to the deviatoric contributions. The dynamic pressure provides the dominant contribution to the dynamic surface topography (Fig. 4) and hence there will be a correspondence between flow-induced stress and surface undulations, where the latter will in a sense represent effective 'bending stresses' acting on the surface. The

horizontal traction vectors (Fig. 6a) are strongly correlated to the horizontal flow directions in the transition zone region of the upper mantle (Fig. 5c). The tractions show a clear convergence below the central U.S., in response to the downwelling driven by the descent of the Farallon slab (Forte et al. 2007). The mean (horizontally averaged) amplitude of the horizontal tractions under North America is nearly 2 MPa and below the western U.S. the regional amplitudes are twice as large and they are directed east-north-east. The same is true of the tractions exerted under western Canada, adjacent to the Juan de Fuca subduction zone.

An alternative and more standard measure of the stress state is provided by predictions of flow induced maximum horizontal compressive stress, $\mathrm{SH}_{\mathrm{max}}$, acting at the base of the lithosphere (Fig. 6b). We note substantial variations, involving an overall rotation of the $\mathrm{SH}_{\mathrm{max}}$ axes, between the eastern and western coastal margins of North America. This spatial variability is dependent on two main factors: (1) the focussed, regional-scale expression of mantle flow driven by the Farallon slab structure in the deep transition-zone region of the upper mantle (Fig. 4c) and, (2) the low sub-lithospheric viscosity inferred from joint convection and glacial rebound data (Fig. 1a). The mean amplitude of $\mathrm{SH}_{\mathrm{max}}$ under North America at the base of the lithosphere is about 9 MPa, including both dynamic pressure and deviatoric stresses. The predicted stress azimuths are in accord with those obtained in previous global flow models (Steinberger et al. 2001; Lithgow-Bertelloni & Guynn 2004) and they are in good agreement with the large-scale pattern of $\mathrm{SH}_{\mathrm{max}}$ in North America given by the World Stress Map Project (Zoback 1992).

The mean amplitudes of the horizontal tractions and stress under North America are similar to those obtained from independent analyses of seismic anisotropy (Bokelmann & Silver 2002) and from mechanical models of the lithosphere (Liu & Bird 2002). The nature of the predicted tractions is clearly 'active', since they are produced by buoyancy driven mantle flow acting on the lithosphere and not vice-versa, in accord with the results of mechanical modelling (Liu & Bird 2002).

The importance of deep mantle buoyancy for the lithospheric stress field may again be explored by carrying out a mantle flow calculation in which all density perturbations in the top 400 km of the mantle have been set to zero. The resulting tractions and compressive stresses (Fig. 6c,d) are

almost identical to the previous predictions (Fig. 6a,b). The horizontal traction and $\mathrm{SH}_{\max}$ fields predicted with zero buoyancy in the upper 400 km (Fig. 6c,d) explain, respectively, over 90% and 50% (expressed in variance reduction) of the corresponding predictions (Fig. 6a,b) obtained with all mantle buoyancy sources.

## 6 EXPLORING THE IMPORTANCE OF LATERAL VISCOSITY VARIATIONS BELOW NORTH AMERICA

The surface plates, which are arguably the most extreme manifestation of lateral rheology variations, were incorporated into the flow calculations presented above. These calculations assumed, however, a 1-D radial variation of viscosity in the mantle and the question therefore arises as to the importance of neglecting lateral viscosity variations (LVV) in sub-lithospheric regions. We will explore here the possible impact of these LVV using a mantle flow model recently developed by Moucha et al. (2004, 2007). This numerical model, called 'VariFlow', is based on a spectral variational formulation of buoyancy induced flow (Forte & Peltier 1994) and it has been extensively benchmarked against another independently derived convection code, called 'CitcomS' (Zhong et al. 2000), which is also designed to deal with LVV. The flow modelling carried out above includes rigid surface plates whose motions are coupled to the underlying mantle flow, but VariFlow is currently implemented with free-slip boundary conditions and therefore does not include dynamically coupled surface plates. Despite this restriction (which will be relaxed in future work), Variflow nonetheless provides a robust means of determining the dynamical consequences of large amplitude LVV throughout the mantle. Although VariFlow provides semi-analytic flow solutions on a global scale (for full details see Moucha et al. 2007), the focus here will be on the detailed dynamics below the North American continent.

The LVV in the mantle were estimated using a classic homologous temperature scaling (Weertman, 1970):

$$\nu = \nu_o \exp\left[\gamma \, \frac{T_{melt}}{T(r,\theta,\phi)}\right] \tag{5}$$

where the factor $\gamma$ relates the creep activation enthalpy to the melting temperature $T_{melt}$, and

the 3-D temperature distribution in the mantle, $T(r, \theta, \phi)$, is derived from seismic tomography models. For simplicity, melting temperatures of 2000 K for the upper-mantle and 4260K for the lower-mantle are assumed, based on the study of Zerr et al. (1998). A constant value of 10 was employed for $\gamma$, to ensure an exact spectral description of the LVV up to harmonic degree 32. For comparison, Karato & Karki (2001) used $\gamma = 10, 20$ in their analysis of the impact of temperature on seismic anelasticity in the lower mantle.

The lateral temperature variations $T(r, \theta, \phi)$ in (5) was constructed from two tomography models: In the upper mantle, lateral temperature variations derived by Forte & Perry (2000) are employed and, for the lower mantle, the lateral temperature variations derived in Forte & Mitrovica (2001) are used. The resulting LVV are then superimposed on a radial viscosity profile (Fig. 7a, blue curve) that increases smoothly with depth to ensure that the viscosity heterogeneity is accurately integrated at all depths by VariFlow. (An analysis of more complicated radial variations in mean viscosity may be found in Moucha et al. 2007.) The full 3-D distribution of viscosity, summarised below in Fig. 7a, exhibits a three order of magnitude variation in the LVV (shaded region) which is comparable to the increase with depth of the horizontally averaged viscosity (blue curve). At 150 km depth, the LVV below North America (Fig. 7b) show a two order of magnitude increase from the southwestern edge of the continent to the central Canadian shield.

The 1-D radial viscosity profiles derived from geodynamic inversions (Mitrovica & Forte 2004) should be interpreted in terms of the horizontally averaged logarithm of the 3-D viscosity distribution (Moucha et al. 2007). To explore the impact of LVV, two separate flow calculations were carried out: Firstly, using the 1-D radial viscosity based on the mean logarithm (Fig. 7a, red dashed curve) and secondly using the full 3-D viscosity structure (Fig. 7a, grey shaded region). In both flow calculations the internal buoyancy forces are derived from the shear velocity anomalies in tomography model TX05WM (Fig. 2) using the geodynamically inferred velocity-density scaling (Fig. 3, solid red and blue curves).

Dynamic topography of North America predicted by both flow models (Fig. 7c, for the 1-D viscosity profile and Fig. 7d, for the 3-D viscosity distribution) shows little impact from large scale LVV. This is an important observation since the dynamic topography is a mapping of flow

induced (vertical) stresses acting on the surface. The stress field is therefore not very sensitive to large scale LVV and the basic physical reason for their apparent internal 'cancellation' has been discussed previously (Forte & Peltier 1994). The predicted flow fields (Fig. 7e,f) show a somewhat larger effect from LVV but it is nonetheless clear that the dominant pattern of east-northeast flow in the asthenosphere below the western half of the continent is robust. Similarly robust is the pattern of convergent horizontal flow, and associated downward flow, below the central U.S. The signature of the subducting Farallon slab in the lower mantle is clearly discernible in the asthenospheric flow field below North America.

## 7 DISCUSSION

The viscous flow model presented here provides a successful match to a broad suite of surface constraints on the dynamics of the North American continent. A key ingredient in this model, which has a fundamental impact on the predicted surface observables and upper-mantle flow, is the incorporation of rigid tectonic plates whose motions are coupled to the underlying viscous flow in the mantle (Forte & Peltier 1994) rather than imposed a-priori. The buoyancy driven flow below the plates, and away from plate boundaries, effectively senses a local no-slip surface and hence is strongly stabilised relative to the standard assumption of free-slip conditions. This stability, in concert with the inferred positive buoyancy of the upper half of the continental roots, has a major impact on the near-surface flow field below North America.

Two key ingredients in this new model of mantle dynamics below North America are the revised estimates of chemical buoyancy in the tectosphere (compared to previous inferences in Perry et al. 2003) and the most recent inferences of mantle viscosity derived by jointly inverting glacial isostatic adjustment and convection-related surface data (Mitrovica & Forte 2004). With this mantle flow model we are able to map out the flow and stresses below the continent at all locations and to greater depth than has been explored to date. In addition to satisfying the major geodynamic observables (gravity, topography, plate motions), our model is also able to successfully reconcile the limited estimates of North American stress and deformation inferred in previous studies.

Our predictions highlight the fundamental importance of deep-mantle buoyancy in understand-

ing the large scale dynamics of the North American continent. The descent of the Kula-Farallon plates within the lower mantle, as well as upwelling below the Pacific Ocean, have a strong, indeed dominant, signature in surface observables such as dynamic topography, gravity, plate motions and stresses. Perhaps surprisingly, this impact is evident even on regional scales. In a recent study we have shown, for example, that downwelling flow dynamically coupled to the descent of the Farallon plate is the driving force responsible for the intra-continental deformation and dynamics below the central U.S. (Forte et al. 2007).

## REFERENCES

Alvarez, W., 1982. Geological evidence for the geographical pattern of mantle return flow and the driving mechanism of plate tectonics, *J. geophys. Res.*, **148**, 6697–6710.

Alvarez, W., 2001. Eastbound sublithosphere mantle flow through the Caribbean gap and its relevance to the continental undertow hypothesis, *Terra Nova*, **13**, 333–337.

Argus, D.F. & Gordon, R.G., 1991. No-net-rotation model of current plate velocities incorporating plate motion model NUVEL-1, *Geophys. Res. Lett.*, **18**, 2039–2042.

Bechtel, T.D., Forsyth, D.W., Sharpton, V.L. & Grieve, R.A.F., 1990. Variations in effective elastic thickness of the North American lithosphere, *Nature*, **343**, 636–638.

Becker, T.W., Schulte-Pelkum, V., Blackman, D.K., Kellogg, J.B. & R.J. O'Connell, 2006. Mantle flow under the western United States from shear wave splitting, *Earth planet. Sci. Lett.,* , **247**, 235–251.

Bird, P., 1998. Testing hypotheses on plate-driving mechanisms with global lithosphere models including topography, thermal structure, and faults, *J. geophys. Res.*, **103**, 10115–10130.

Bokelmann, G.H.R., 2002a. Which forces drive North America? *Geology*, **30**, 1027–1030.

Bokelmann, G.H.R., 2002b. Convection-driven motion of the North American continent: Evidence from P-wave anisotropy, *Geophys. J. Int.*, **248**, 278–287.

Bokelmann, G.H.R. & Silver, P.G., 2002. Shear stress at the base of shield lithosphere, *Geophys. Res. Lett.*, **29**, 6–1.

Bunge, H.-P. & Grand, S.P., 2000. Mesozoic plate-motion history below the northeast Pacific Ocean from seismic images of the subducted Farallon slab, *Nature*, **405**, 337–340.

Cammarano, F., Goes, S., Vacher, P., & Giardini, D., 2003. Inferring upper-mantle temperatures from seismic velocities, *Phys. Earth Planet. Int.*, **138**, 197–222.

Canil, D., Schulze, D.J., Hall, D., Hearn Jr., B.C. & Milliken S.M., 2003. Lithospheric roots beneath western Laurentia: the geochemical signal in mantle garnets, *Can. J. Earth Sci.*, **40**, 1027–1051.

Dixon, J.E., Dixon, T.H., Bell, D.R. & Malservisi, R., 2004. Lateral variation in upper mantle viscosity: Role of water, *Earth Planet. Sci. Lett.*, **222**, 451–467.

Du, W.-X., Kim, W.-Y. & Sykes, L.R., 2003. Earthquake source parameters and state of stress for the northeastern United States and southeastern Canada from analysis of regional seismograms, *Bull. Seis. Soc. Am.*, **93**, 1633–1648.

Flesch, L.M., Holt, W.E., Haines, A.J. & Bingming, S.-T., 2000. Dynamics of the Pacific-North American plate boundary in the western United States, *Science*, **287**, 834–836.

Forte, A.M., 2007. Constraints on seismic models from other disciplines – Implications for mantle dynamics and composition, in Volume 1 of *Treatise of Geophysics*, edited by B. Romanowicz & A.M. Dziewonski, Elsevier, pp. 805–858.

Forte, A.M. & Grand, S.P., 2003. Constraints on vertical flow between the upper and lower mantle from simulations inversions of global seismic and geodynamic data, *Geophys. Res. Abstracts* (EGS), **5**, No. 14070.

Forte, A.M. & Mitrovica, J.X., 2001. Deep-mantle high-viscosity flow and thermochemical structure inferred from seismic and geodynamic data, *Nature*, **410**, 1049–1056.

Forte, A.M. & Peltier, W.R., 1987. Plate tectonics and aspherical Earth structure: The importance of poloidal–toroidal coupling. *J. geophys. Res.*, **92**, 3645–3679.

Forte, A.M. & Peltier, W.R., 1991. Viscous flow models of global geophysical observables 1. Forward problems, *J. geophys. Res.*, **96**, 20131–20159.

Forte, A.M. & Peltier, W.R., 1994. The kinematics and dynamics of poloidal-toroidal coupling in mantle flow: The importance of surface plates and lateral viscosity variations, *Adv. Geophys.*, **36**, 1–119.

Forte, A.M. & Perry, H.K.C., 2000. Geodynamic evidence for a chemically depleted continental tectosphere, *Science*, **290**, 1940–1944.

Forte, A.M., J.X. Mitrovica, R. Moucha, N.A. Simmons, S.P. Grand, 2007. Descent of the ancient Farallon slab drives localised mantle flow below the New Madrid seismic zone, *Geophys. Res. Lett.,* , **34**, L04308, doi:10.1029/2006GL027895.

Fouch, M.J., Fischer, K.M., Parmentier, E.M., Wysession, M.E. & Clarke, T.J., 2000. Shear wave splitting, continental keels, and patterns of mantle flow, *J. geophys. Res.*, **105**, 6255–6276.

Gable, C.W., O'Connell, R.J. & Travis, B.J., 1991. Convection in three dimensions with surface plates. *J. geophys. Res.*, **96**, 8391–8405.

Gan, W. & Prescott, W.H., 2001. Crustal deformation rates in central and eastern U.S. inferred from GPS, *Geophys. Res. Lett.*, **28**, 3733–3736.

Godey, S., Snieder, R., Villaseor, A. & Benz, H.M., 2003. Surface wave tomography of North America and the Caribbean using global and regional broad-band networks: phase velocity maps and limitations of ray theory, *Geophys. J. Int.*, **152**, 620–632.

Godey, S., Deschamps, F., Trampert, J. & Snieder, R., 2004. Thermal and compositional anomalies beneath the North American continent, *J. geophys. Res.,* , **109**, B01308, doi:10.1029/2002JB002263.

Goes, S. & van der Lee, S., 2002. Thermal structure of the North American uppermost mantle inferred from seismic tomography, *J. geophys. Res.*, **107**, ETG 2-1.

Gök, R., Ni, J.F., West, M., Sandvol, E., Wilson D., Aster, R., Baldridge, W.S., Grand, S., Gao, W., Tillmann, F. & Semken, S., 2003. Shear wave splitting and mantle flow beneath LA RISTRA, *Geophys. Res. Lett.*, **30**, 16–1.

Gough, D.I., Fordjor, C.K. & Bell, J.S., 1983. A stress province boundary and tractions on the North American plate, *Nature*, **305**, 619–621.

Gough, D.I., 1984. Mantle upflow under North America and plate dynamics, *Nature*, **311**, 428–433.

Grand, S.P., 1994. Mantle shear structure beneath the Americas and surrounding oceans, *J. geophys. Res.*, **99**, 11591–11622.

Grand, S.P., van der Hilst, R.D. & Widiyantoro, S., 1997. Global seismic tomography: a snapshot of convection in the Earth, *GSA Today*, **7**, 1–7.

Gurnis, M., 1988. Large-scale mantle convection and the aggregation and dispersal of supercontinents, *Nature*, **332**, 695–699.

Hager, B. H. & Clayton, R. W., 1989. Constraints on the structure of mantle convection using seismic observations, flow models, and the geoid. In *Mantle Convection: Plate tectonics and global dynamics* (ed. W. R. Peltier), pp. 657–763. New York: Gordon and Breach.

Hoffman, P.F., 1988. United Plates of America, the birth of a craton: Early proterozoic assembly and growth of Laurentia, *Ann. Rev. Earth Planet. Sci.*, **16**, 543–603.

Hoffman, P.F., 1990. Geological constraints on the origin of the mantle root beneath the Canadian Shield, *Phil. Trans. Roy. Soc. London A*, **331**, 523–532.

Jordan, T.H., 1975. The continental tectosphere, *Rev. Geophys. Space Phys.*, **13**, 1–12.

Jordan, T.H., 1978. Composition and development of the continental tectosphere, *Nature*, **274**, 544–548.

Jordan, T.H., 1981. Continents as a chemical boundary layer, *Phil. Trans. Roy. Soc. London A*, **301**, 359–373.

Jung, H. & Karato, S.-I., 2001. Water-induced fabric transitions in olivine, *Science*, **293**, 1460–1463.

Kaban, M.K., Schwintzer, P., Artemieva, I.M. & Mooney, W.D., 2003. Density of the continental roots: compositional and thermal contributions, *Earth Planet. Sci. Lett.*, **209**, 53–69.

Kaminski, É. & Ribe, N.M., 2001. A kinematic model for recrystallization and texture development in olivine polycrystals, *Earth Planet. Sci. Lett.*, **189**, 253–267.

Karato, S.-I. & Karki, B.B., 2001. Origin of lateral variation of seismic wave velocities and density in the deep mantle, *J. geophys. Res.*, **106**, 21771–21784.

Kauffman, E.G., 1988. Concepts and Methods of High-Resolution Event Stratigraphy, *Ann. Rev. Earth.*

*Planet. Sci.*, **16**, 605–654.

Lithgow-Bertelloni, C. & Gurnis, M., 1997. Cenozoic subsidence and uplift of continents from time-varying dynamic topography, *Geology*, **25**, 735–738.

Lithgow-Bertelloni, C. & Richards, M.A., 1998. The dynamics of Cenozoic and Mesozoic plate motions, *Rev. Geophys.*, **36**, 27–78.

Lithgow-Bertelloni, C. & H. Guynn, J.H., 2004. Origin of the lithospheric stress field, *J. geophys. Res.*, **109**, B01408-32pp.

Liu, Z. & Bird, P., 2002. North America plate is driven westward by lower mantle flow, *Geophys. Res. Lett.*, **29**, 17–1.

Lowman, J.P. & Jarvis, G.T., 1999. Effects of mantle heat source distribution on supercontinent stability, *J. geophys. Res.*, **104**, 12733–12746.

Mitrovica, J.X. & Forte, A.M., 2004. A new inference of mantle viscosity based upon joint inversion of convection and glacial isostatic adjustment data, *Earth Planet. Sci. Lett.*, **225**, 177–189.

Mitrovica, J.X., Beaumont, C. & Jarvis, G.T., 1989. Tilting of continental interiors by the dynamical effects of subduction, *Tectonics*, **8**, 1079–1094.

Moucha, R., Forte, A.M., Mitrovica, J.X. & Daradich A., 2004. Geodynamic implications of convection-related surface observables: The role of lateral variations in mantle rheology, *Eos Trans. AGU*, **85**(47), Fall Meet. Suppl., Abstract T11E–1325.

Moucha, R., Forte, A.M., Mitrovica, J.X. & Daradich A., 2007. Lateral variations in mantle rheology: Implications for convection related surface observables and inferred viscosity models, *Geophys. J. Int.*, **169**, 113-135.

Moucha, R., Forte, A.M., Rowley, D.B., Mitrovica, J.X., Simmons, N.A., Grand, S.P., 2008. Mantle convection and the recent evolution of the Colorado Plateau and the Rio Grande rift valley, *Geology*, **36**(6), 439-442.

Nettles, M. & Dziewonski, A.M., 2008. Radially anisotropic shear velocity structure of the upper mantle globally and beneath North America, *J. geophys. Res.,* , **113**, B02303, doi:10.1029/2006JB004819.

Pari, G. & Peltier, W.R., 2000. Subcontinental mantle dynamics: A further analysis based on the joint constraints of dynamic surface topography and free-air gravity, *J. geophys. Res.*, **105**, 5635–5662.

Perry, H.K.C., Eaton, D.W.S. & Forte, A.M., 2002. LITH5.0: a revised crustal model for Canada based on Lithoprobe results, *Geophys. J. Int.*, **150**, 285–294.

Perry, H.K.C., Forte, A.M. & Eaton, D.W.S., 2003. Upper-mantle thermochemical structure below North America from seismic-geodynamic flow models, *Geophys. J. Int.*, **154**, 279–299.

Poudjom Djomani, Y.H., O'Reilly, S.Y., Griffin, W.L. & Morgan, P., 2001. The density structure of subcontinental lithosphere through time, *Earth Planet. Sci. Lett.*, **184**, 605–621.

Ricard, Y., Fleitout, L. & Froidevaux, C.,1984. Geoid heights and lithospheric stresses for a dynamic Earth

*Ann. Geophys.*, **2**, 267–286.

Ricard, Y. & Vigny, C., 1989. Mantle dynamics with induced plate tectonics, *J. geophys. Res.*, **94**, 17543–17559.

Richards, M.A. & Hager, B.H., 1984. Geoid anomalies in a dynamic earth, *J. geophys. Res.*, **89**, 5987–6002.

Richardson, R.M. & Reding, L.M., 1991. North American plate dynamics, *J. geophys. Res.*, **96**, 12201–12223.

Rudnick, R.L., McDonough, W.F. & O'Connell, R.J., 1998. Thermal structure, thickness and composition of continental lithosphere, *Chem. Geol.*, **145**, 395–411.

Russell, J.K. & Kopylova, M.G., 1999. A steady state conductive geotherm for the north central Slave, Canada: Inversion of petrological data from the Jericho Kimberlite pipe, *J. geophys. Res.*, **104**, 7089–7102.

Silver, P.G. & Chan, W.W., 1991. Shear wave splitting and subcontinental mantle deformation, *J. geophys. Res.*, **96**, 16429–16454.

Silver, P.G. & Holt, W.E., 2002. The mantle flow field beneath western North America, *Science*, **95**, 1054–1058.

Simmons, N., A.M. Forte, and S.P. Grand, 2006. Constraining mantle flow with seismic and geodynamic data: A joint approach, *Earth planet. Sci. Lett.,* , **246**, 109–124.

Sleep, N.H., 2005. Evolution of the continental lithosphere, *Ann. Rev. Earth Planet. Sci.*, **33**, 369–393.

Steinberger, B., Schmeling, H., & Marquart, G., 2001. Large-scale lithospheric stress field and topography induced by global mantle circulation, *Earth Planet. Sci. Lett.*, **186**, 75–91.

van der Lee, S. & Nolet, G., 1997. Upper mantle S velocity structure of North America, *J. geophys. Res.*, **102**, 22815–22838.

Weertman, J., 1970. The creep strength of the earth's mantle, *Rev. Geophys. Space Phys.*, **8**, 145–168.

Zandt, G., Gilbert, H., Owens, T.J., Ducea, M., Saleeby, M.J. & Jones, C.H., 2004. Active foundering of a continental arc root beneath the southern Sierra Nevada in California, *Nature*, **431**, 41–46.

Zerr, A., Diegeler, A. & Boehler, R., 1998. Solidus of Earth's Deep Mantle, *Science*, **281**, 243–246.

Zhong, S., Zuber, M.T., Moresi, L. & Gurnis, M., 2000. Role of temperature-dependent viscosity and surface plates in spherical shell models of mantle convection, *J. geophys. Res.*, **105**, 11063–11082.

Ziegler, A.M., Rowley, D.B., Lottes, A.L., Sahagian, D.L., Hulver, M.L. & Gierlowski, T.C., 1985. Paleogeographic Interpretation: With an example from the mid-Cretaceous, *Ann. Rev. Earth Planet. Sci.*, **13**, 385–428.

Zoback, M.L. & Zoback, M., 1980. State of stress in the conterminous United States, *J. geophys. Res.*, **85**, 6113–6156.

Zoback, M.L., 1992. First- and second-order patterns of stress in the lithosphere - The World Stress Map project, *J. geophys. Res.*, **97**, 11703–11728.

**Table 1:** Fit[1] Between Predicted[2] and Observed[3] Geodynamic Data

| Mantle Density Model | *North American Free-Air Gravity* | *North American Dynamic Topography* | *North American Surface Velocity* | *Global Free-Air Gravity Anomalies* | *Global Dynamic Surface Topography* | *Global Surface Plate Velocities* |
|---|---|---|---|---|---|---|
| *Inverted* ¶ | 71% (13.6 *mGal*) | 60% (685 *m*) | 96% (3.9 *cm/a*) | 73% (13.4 *mGal*) | 54% (665 *m*) | 95% (4.1 *cm/a*) |
| *Isopycnic Hypothesis* * | 70% (13.4 *mGal*) | 54% (659 *m*) | 96% (4.0 *cm/a*) | 72% (13.4 *mGal*) | 48% (641 *m*) | 96% (4.1 *cm/a*) |
| $\delta\rho > 400$ *km*† | 73% (13.0 *mGal*) | 37% (471 *m*) | 92% (3.4 *cm/a*) | 72% (12.6 *mGal*) | 28% (505 *m*) | 92% (3.4 *cm/a*) |
| $\delta\rho > 670$ *km*‡ | 64% (11.3 *mGal*) | 32% (471 *m*) | 69% (2.4 *cm/a*) | 61% (11.1 *mGal*) | 20% (446 *m*) | 68% (2.4 *cm/a*) |
| $\delta\rho < 670$ *km*§ | 20% (5.2 *mGal*) | 46% (387 *m*) | 57% (1.9 *cm/a*) | 23% (5.8 *mGal*) | 47% (419 *m*) | 57% (2.3 *cm/a*) |

*1* Fits are expressed in terms of percent variance reduction.

*2* Root-mean-square (rms) amplitudes are shown in parentheses below the variance reductions. All predictions are obtained on the basis of the geodynamic kernels in Fig. 1 and the tomography model TX05WM (Fig. 2).

*3* All data sets are described in Perry et al. (2003).

¶ Mantle density from inverted dlnρ/dlnVs in Fig. 3 (solid red and blue curves).

* Mantle density from inverted dlnρ/dlnVs in Fig. 3 (dashed red and blue curves).

† For depth $z < 400$ km, density anomalies $\delta\rho = 0$ (for $z > 400$ km, $\delta\rho$ from inverted¶ dlnρ/dlnVs ).

‡ For depth $z < 670$ km, density anomalies $\delta\rho = 0$ (for $z > 670$ km, $\delta\rho$ from inverted¶ dlnρ/dlnVs).

§ For depth $z > 670$ km, density anomalies $\delta\rho = 0$ (for $z < 670$ km, $\delta\rho$ from inverted¶ dlnρ/dlnVs).

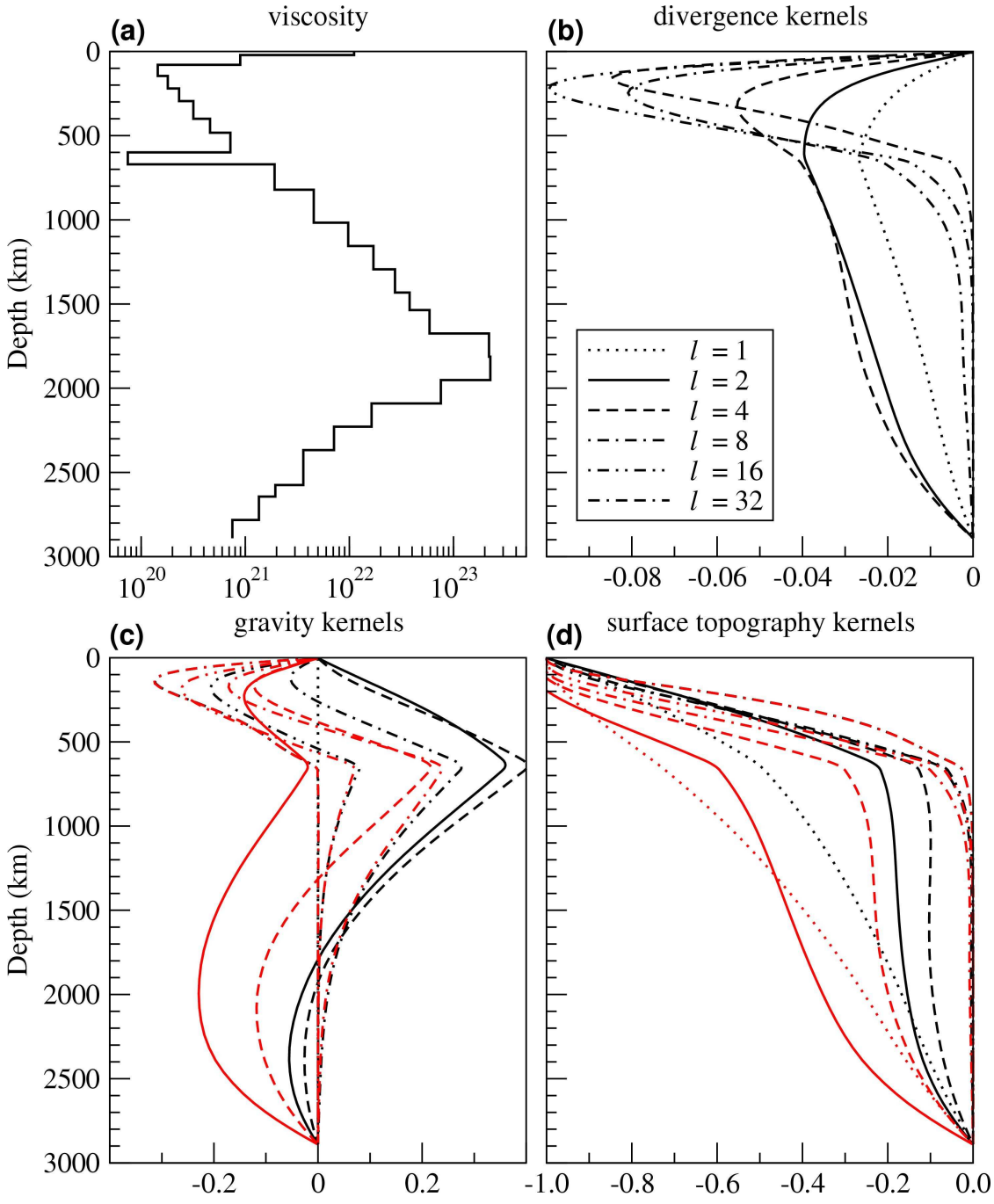


**Figure 1.** Mantle viscosity and geodynamic response functions. (a) The depth variation of mantle viscosity derived from a nonlinear iterative joint inversion of mantle convection data (in Table 1) and GIA data (Mitrovica & Forte 2004). Absolute values of viscosity (in units of $10^{21}$ Pa s) are plotted. The geodynamic response or kernel functions shown here (frames b – d) are calculated on the basis of the viscosity profile shown in frame (a). The horizontal divergence kernels are shown in frame (b). The gravity kernels for free-slip (black lines) and no-slip (red lines) surface boundary conditions are shown in frame (c). The dynamic topography kernels for free-slip (black lines) and no-slip (red lines) conditions are shown in frame (d). In all frames the kernels corresponding to harmonic degrees $\ell = 1, 2, 4, 8, 16, 32$ are identified by the legend in frame (b).

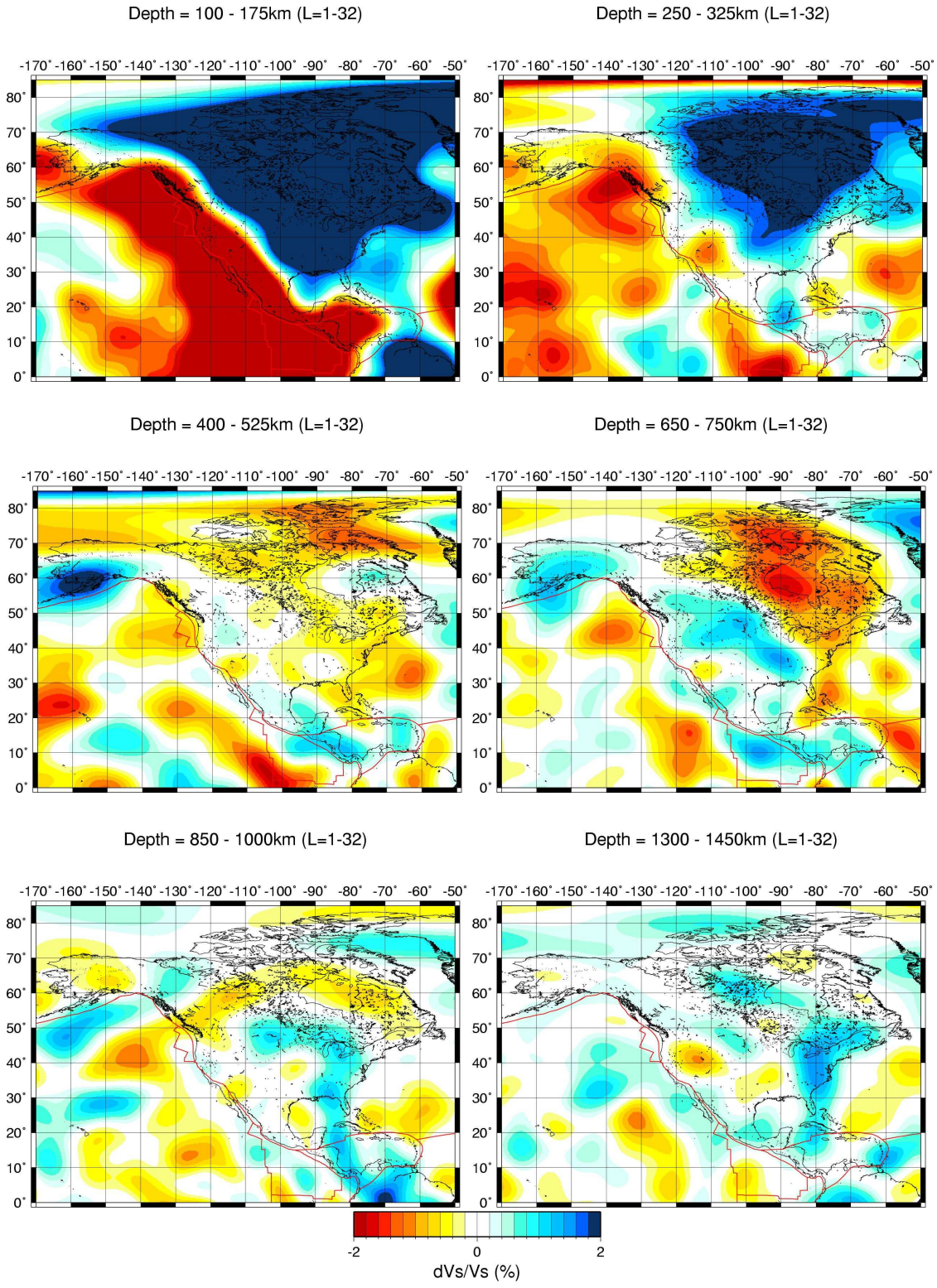


**Figure 2.** Mantle structure below North America. Shown here are maps of relative perturbations of seismic shear velocity $\delta V_S/V_S$ (scale shown at bottom of figure) obtained from the high-resolution seismic tomography model TX05WM (Simmons et al. 2006). All maps have been synthesized from a spherical harmonic expansion of the seismic anomalies which is truncated at degree $\ell = 32$. Since the same colour scale (bottom of figure) is used for all depths, a saturation of the colours occurs when the amplitude of the anomalies exceeds $\pm 2\%$ at shallow depths (top two maps).

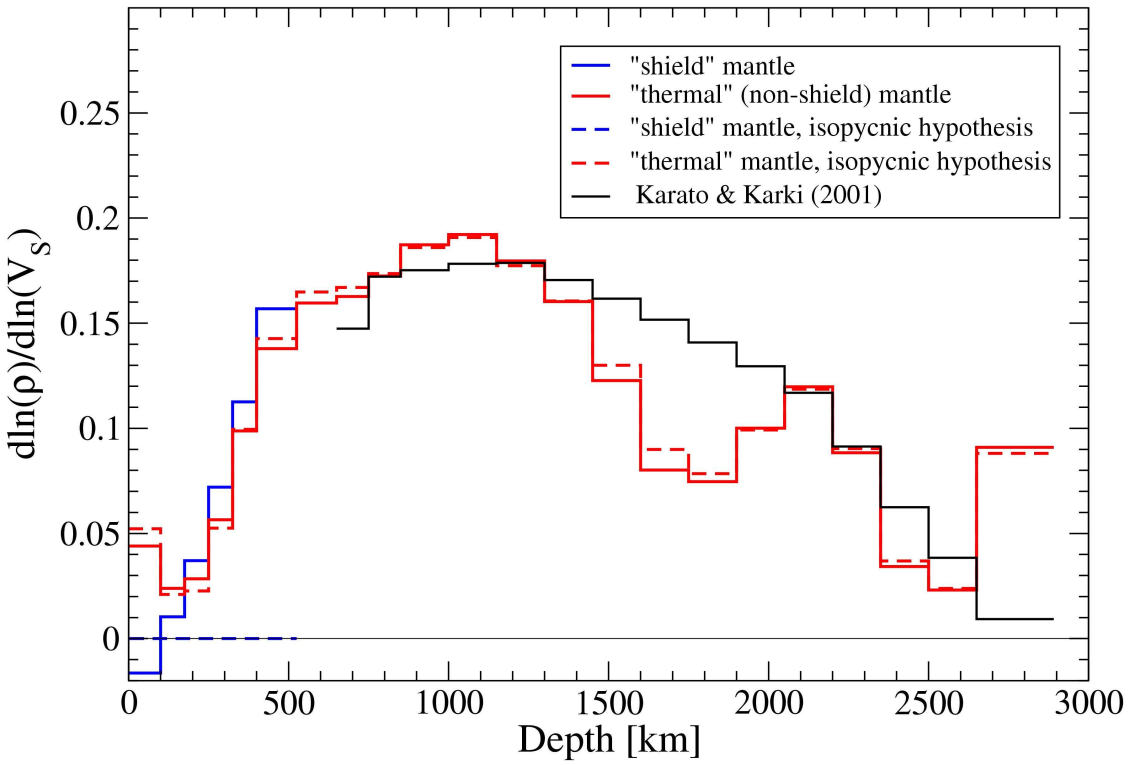


**Figure 3.** Geodynamic inference of mantle density structure. The solid black line represents the $\mathrm{dln}\,\rho/\mathrm{dln}\,\mathrm{V_S}$ (velocity-to-density) scaling coefficient estimated on the basis of mineral physics data (Karato & Karki 2001), assuming that lower-mantle density and seismic shear velocity anomalies are thermal in origin. The solid blue and red lines represents the Occam-inferred scaling coefficients for the mantle below the continental shield, where $\delta V_S = (\delta V_S)_{shield} > 0$, and for the ambient ('thermal' or non-shield) mantle, where $\delta V_S = (\delta V_S)_{thermal}$, respectively. The dashed red line is the inferred scaling coefficient for 'thermal' mantle assuming that the isopycnic hypothesis (Jordan 1978) is valid, in which case $(\delta\rho)_{shield} = 0$ and hence $(\mathrm{dln}\,\rho/\mathrm{dln}\,\mathrm{V_S})_{\mathrm{shield}} = 0$ (dashed blue line). All density inversions employed viscous response functions in Fig. 1 and they are based on the shear velocity tomography model TX05WM in Fig. 2.

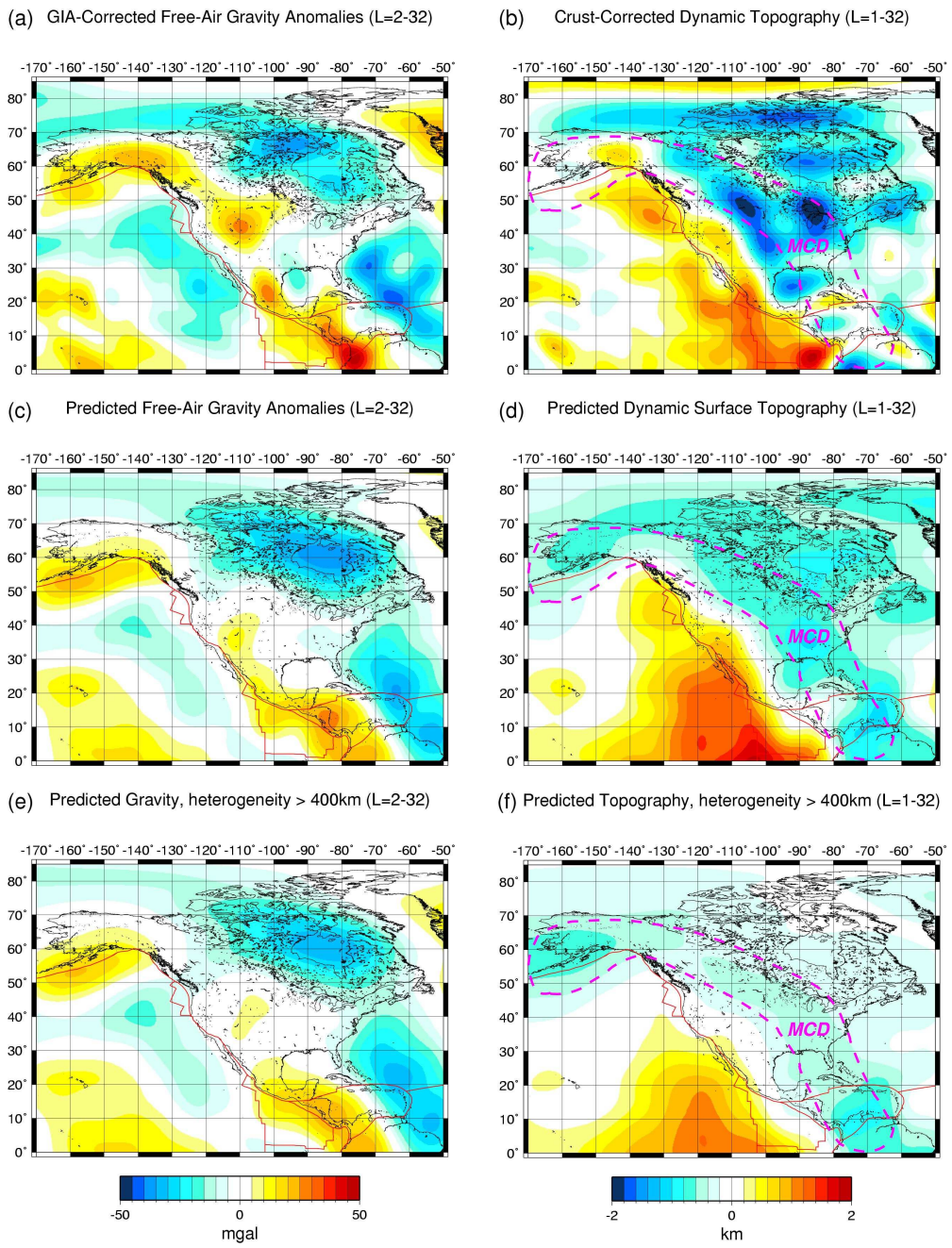


**Figure 4.** North American free-air gravity and topography anomalies. The observed free-air gravity and topography anomalies have been corrected for the effects of isostatically compensated crustal heterogeneity and GIA contributions (see Perry et al. 2003 for details) and the residual, nonhydrostatic fields are plotted in (a) and (b) respectively. All fields (a-f) have been synthesized by summing spherical harmonic coefficients up to degree and order 32. The free-air gravity and dynamic topography fields predicted on the basis of the geodynamic kernels in Fig. 1 and using tomography model TX05WM (Fig. 2) are shown in (c) and (d) respectively. Maps (e) and (f) show the gravity and topography predicted by the viscous flow model when all density anomalies in the upper 400 km of the mantle are set to zero. The viscous flow predictions (c-f) employ the velocity-density scaling given by the solid blue and red lines in Fig. 3. The dashed magenta curve superimposed on the dynamic topography maps (b,d,f) encloses the mid-continental depression (MCD) which overlies the descending Kula-Farallon lithospheric plates in the lower mantle.

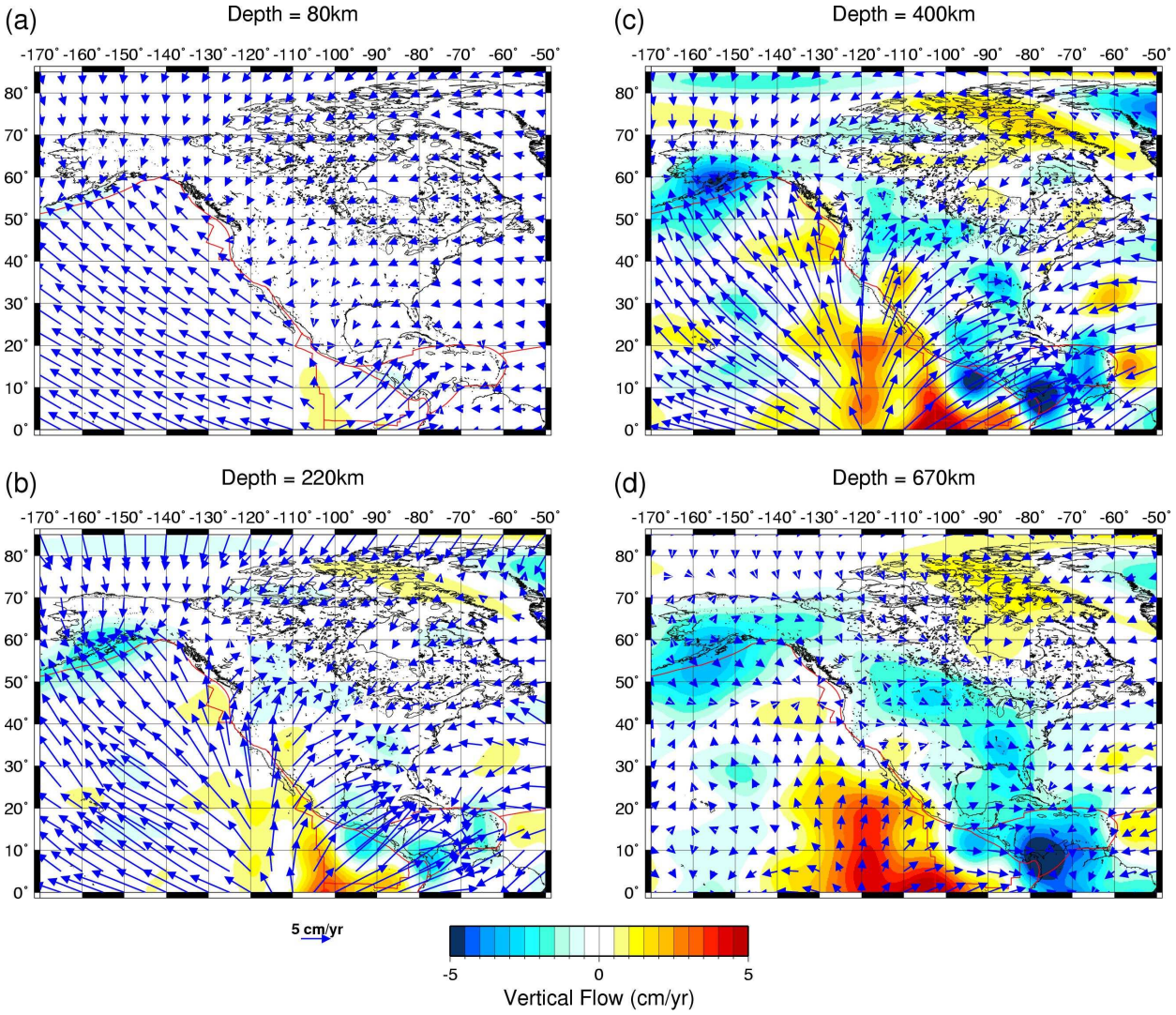


**Figure 5.** Predicted mantle flow below North America. Rates of horizontal (blue arrows) and vertical flow (coloured contours) predicted by the tomography-based mantle flow model at depths of (a) 80 km, (b) 220 km, (c) 400 km and (d) 670 km. The viscous flow calculation employs the tomography model TX05WM (Fig. 2), the viscosity profile in Fig. 1a, and the density-velocity scaling coefficients represented by the solid blue and red lines in Fig. 3. The horizontal and vertical velocity scale for all maps is centred at the bottom of the figure.

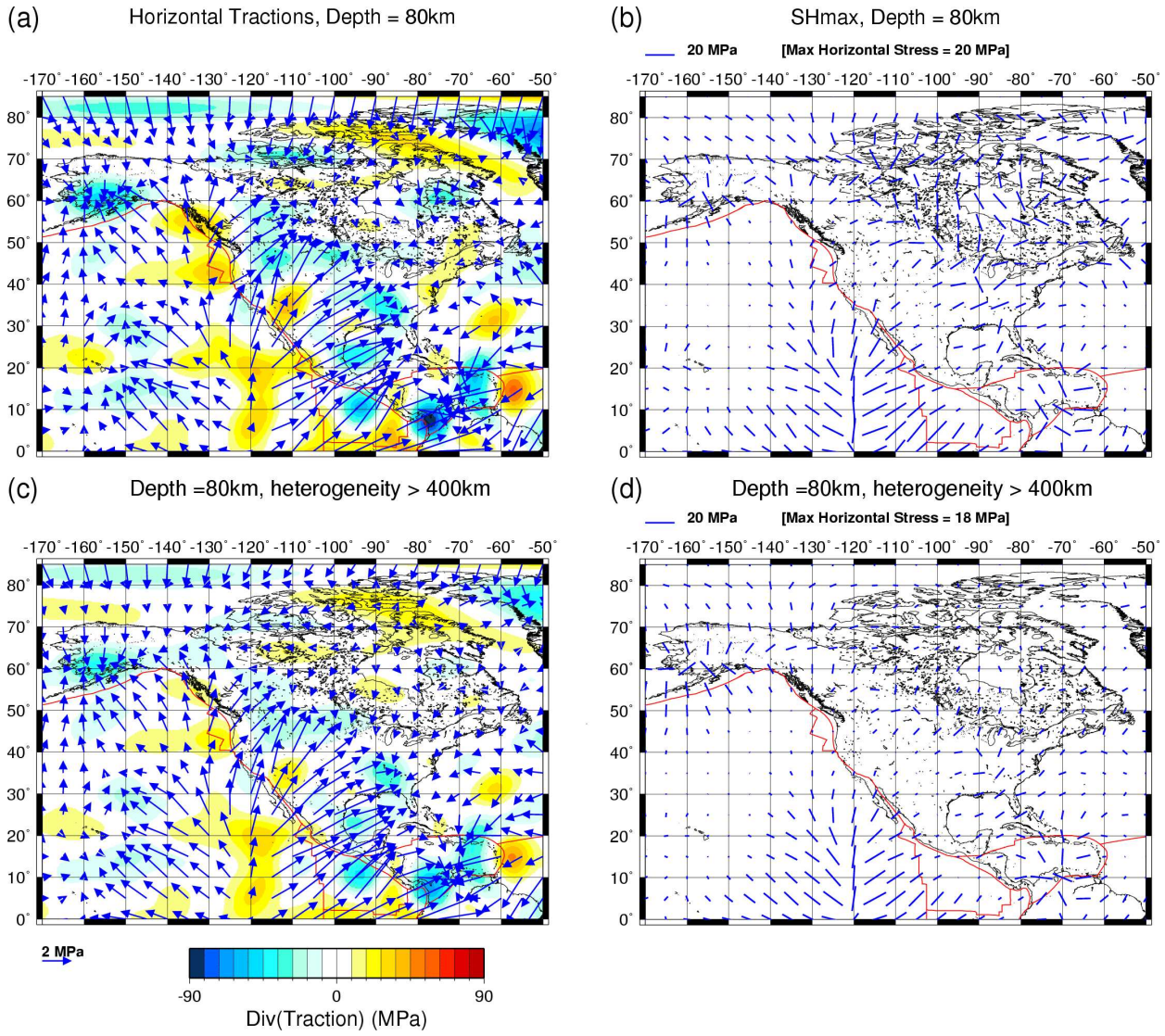


**Figure 6.** Predicted tractions and compressive stresses acting on North American lithosphere. (a) Predicted horizontal components of the flow-induced traction acting at the base of the lithosphere. The predicted tractions vectors (horizontal scale shown at bottom left of frame c) are derived from the same viscous flow calculation employed in Figs. 4 and 5. The contours (scale shown at bottom of frame c) represent the horizontal divergence (yellow-red colours) and convergence (green-blue colours) of the traction field. (b) Predicted maximum horizontal compressive stress, $SH_{max}$, at the base of the lithosphere (scale shown at top left of map). In (c) and (d) are shown the corresponding predictions when all density anomalies in the top 400 km of the mantle are set to zero.

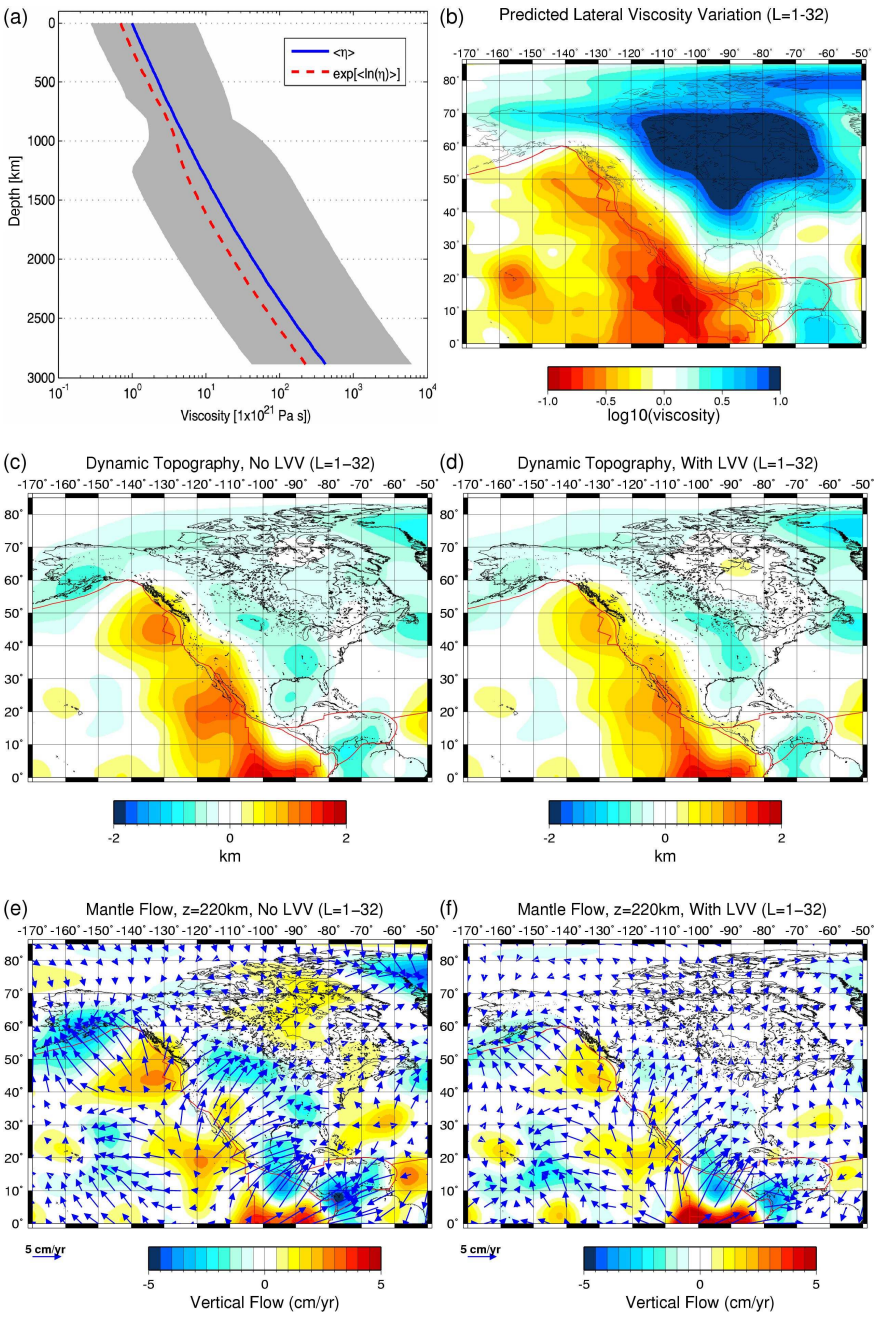


**Figure 7.** Impact of lateral viscosity variations (LVV) on North American mantle dynamics. (a) The shaded grey region shows the dynamic range (min–max) of LVV and the horizontal average value is shown by the solid blue line. The dashed red line shows the horizontal average of the natural logarithm of mantle viscosity. (b) Map of LVV (logarithmic colour scale at bottom) at a depth of 150 km below North America. (c) Dynamic surface topography calculated in the absence of LVV, using the solid blue line in frame (a). (d) Surface topography predicted with the full LVV (shaded area, frame a). (e) Mantle flow at 220 km depth predicted in the absence of LVV, using the absolute viscosity given by the dashed red curve in frame (a). (f) Mantle flow predicted at 220 km depth with full LVV (shaded area, frame a). All topography and flow predictions in maps (c)-(f) are synthesized from spherical harmonics up to degree 32 and they use mantle density anomalies derived from tomography model TX05WM (Fig. 2) and the density-velocity scaling coefficients represented by the solid blue and red lines in Fig. 3.